Luminescent Fe:ZnSe Doped As-S-Se Optical Composites for the Mid-infrared

Rashi Sharma[1], Alexandros Kostogiannes[2], Daniel Wiedman[3], Jaynlynn Sosa[2], Justin Cook[1], James Drake[1], David Furniss[4], Boyu Xiao[4], Angela B. Seddon[4], Parag Banerjee[2], Kenneth L. Schepler[1], Kathleen A. Richardson[1]

[1]CREOL, College of Optics and Photonics, UCF, Orlando, FL, USA
[2]Department of Materials Science and Engineering, UCF, Orlando, Fl, USA
[3]Department of Chemistry, UCF, Orlando, Fl, USA
[4]Mid-Infrared Photonics Group, George Green Institute for Electromagnetics Research, Faculty of Engineering, University of Nottingham, NG7 2RD, UK

ABSTRACT

Active transition metal ion (TM) doped infrared transparent chalcogenide glasses are a promising class of solid-state materials which can be drawn into a new generation of optical fibers for efficient sources of mid-infrared (MIR) lasers. This work evaluates a candidate glass matrix system of As-S-Se chalcogenide glass as a host for iron (Fe) doped ZnSe crystals. Despite good refractive index match between the chalcogenide glass and the Fe^{2+}:ZnSe particles, the stability of the dopant is critically impacted by the melt temperature conditions. To address this issue, Fe^{2+}:ZnSe particles were coated with a conformal shell of Al_2O_3, via Atomic Layer Deposition (ALD), to improve the stability of the dopant in the chalcogenide glass matrix melt environment. An ozone pretreatment of the ZnSe powders prior to ALD also improved particle stability, resulting in significant reduction in dissolution of coated powders. Moreover, an improvement in the drying protocol of the glass resulted in significantly lower impurity concentrations. The broadband optical emission of the composites in the 3520-5200 nm region was measured using Er (III):YAG pump laser. Improved ALD coating and drying protocol resulted in a bulk optical composite with higher emission signal compared to previous composite fabricated without these protocols, for the same loading levels.

Keywords: ZnSe doped chalcogenide glasses, Infrared glass ceramics, MIR fibers

1. INTRODUCTION

High transparency of chalcogenide glasses (ChGs) in the infrared (IR) regime is characterized by the broad glass forming tendency of Group IV, V and VI elements (excluding oxygen). Further optimization of the glass' composition, through composition tailoring, can extend the ChGs use in diverse applications in fields such as environmental, bioengineering, medical and gas sensing [1,2]. Mid-infrared (MIR) laser sources are another application where the intrinsic limitations of low glass transition temperature, limited thermal and mechanical stability, and active optical (luminescence) applications can be overcome. Due to the challenges in achieving population inversion, the production of MIR fiber lasers that emit at wavelengths longer than $\lambda = 4$ μm is extremely difficult with currently available glass fiber sources. To overcome this limitation, efforts have been made to dope a secondary active TM-(transition metal ion)-doped crystallite in the glass by tailoring the broadband refractive index and dispersion properties in chalcogenide composites [3]. Recently, efforts have been made to use such multi-phase (glass + crystallite containing) optical composites towards creating a new laser source in the MIR region [4]. The introduction of nano/micro crystals that employ transition metal ions (TM) as a dopant in a ChG glass matrix has been shown to be promising as a future MIR laser source. The composite's high quantum efficiency, large emission cross-section, broadband emission and absorption bands make them ideal candidates for MIR sources. However, realizing these attributes can prove challenging when trying to align the optical and physical properties of host and dopant.

Prior work has been reported on efforts in which TM-doped chalcogenide glasses were used as a gain medium in the MIR (3-5 μm) region towards use as a femtosecond pulse or tunable lasers [5,6]. As in the case of any active material's loading, the environment observed by the dopant within the glass matrix plays a key role towards developing a stable composite.

Bulk $Fe^{2+:}$ZnSe has been shown to demonstrate lasing in the MIR region due to the strong electron-phonon coupling between the crystalline lattice and active ion [7]. Due to the amorphous nature of glass, similar results could not be achieved with the same dopants due primarily to solubility limits. As noted, it is desirable to have MIR emission in the form of an optical fiber, which can remain stable during laser alignment while also possessing properties compatible with any cooling required to maintain beam quality. Recent efforts to integrate TM ion dopants in the glass ChG media still have not reached the phase stability and loss level of the glass-only media.

In the past, our group has worked with (Fe^{2+}:ZnSe) as the dopant crystallite in a refractive index matched ChG glass matrix. An As-S-Se glass matrix was chosen as a host because of its optical compatibility with the sphalerite-type ZnSe in the (3-5 μm) region, as well as its crystallization stability, a key metric required for potential subsequent fiberization. These attributes have been discussed in prior work reporting the thermomechanical, optical and viscoelastic properties of the glass composite for efficient fiber drawing capabilities and where we evaluated the stability of ZnSe in the glass matrix [8]. Further work has been carried out to enhance stability of the ZnSe during the optical composite process via atomic layer deposition (ALD) followed by an in-depth study of the impact of powder handling on the presence of impurities in the composite [9, 10]. In these early efforts, despite high optical loss due to moisture absorption and scattering from trapped gas (bubbles), as well as low levels of partial dissolution of Fe^{2+}:ZnSe particles in the glass matrix, a strong and broad emission band at 3.5-5.5 μm was observed [11]. This paper is a step towards demonstrating how consistent efforts made to reduce the presence of ZnSe aggregates, and bubbles formed due to ZnSe dissolution via improved ALD processing, powder handling, drying and melt protocols resulted in almost doubling the emission signal strength of the glass composite.

2. EXPERIMENTAL

2.1 Preparation of Fe^{2+}:ZnSe particles

Bulk Fe^{2+}:ZnSe samples were fabricated by researchers at the Air Force Research Laboratory (AFRL) using the hot isostatic pressing (HIP) treatment method [12,13]. To prepare the Fe^{2+}:ZnSe powder, bulk polycrystalline $Fe^{2+:}$:ZnSe ceramic coupons doped with 10^{19} ions/cm^3 Fe^{2+} concentration were ground using a ball mill in ambient lab temperature and humidity and then sieved using a 200 mesh sieve in a MBraun glove box using a sieve shaker (DuraTap™ Sieve Shaker, Advantech). The microparticles with dimensions ≤ 25 μm were used in this work to incorporate in the multicomponent glass matrix. To prevent the dissolution of Fe^{2+}:ZnSe in the host glass matrix during the remelt heat treatment, the Fe^{2+}:ZnSe powder was coated with an alumina shell using an ALD viscous flow reactor. The powder (0.5 g) was placed in a barrel reactor and loaded into the ALD flow reactor. The details of the reactor have been discussed in our previous work and are shown in Figure 1 [9]. The rotating barrel reactor (1.5″ in diameter and 2″ long) was made of 316 steel and is lined with Teflon®. The magnetic drive assembly (Transfer Engineering and Manufacturing Inc.,) rotates the barrel along its cylindrical axis at 24 RPM to enable tumbling of the ZnSe powders and enable coating of all particle surfaces. The barrel has openings in the center on both ends to allow gases to pass through, while preventing powder loss. The powder was treated with ozone gas (Absolute Ozone Nano15) at RT (room temperature) for 30 min (1 torr), after that the temperature of the furnace was raised to 215 °C. Alternate pulses (300 cycles) of trimethylaluminum (TMA) (0.5 s) and deionized (DI) H_2O (1 s) separated with an argon (Ar) purge (75 sccm) for 20 s were used. TMA and DI H_2O were maintained at room temperature. The ALD chamber pressure was kept at < 1 Torr throughout the deposition.

2.2 Sample Fabrication

To fabricate the 94.6 As_2S_3 – 5.4 As_2Se_3 (mol.%) ChG glass used in the optically active composite material, the melt quenching technique was employed [8,9]. This ChG composition was chosen to match both the refractive index and dispersion of ZnSe across the wavelength range of interest as well as its capability to form low-loss optical fibers [8]. High purity (5N) raw materials (As, S, Se) were combined in a fused silica ampoule and evacuated to 10^{-2} Torr before being sealed with a hydrogen/oxygen gas torch. The ampoule was then placed inside a rocking furnace and heated at 1 °C/min up to 750 °C and maintained at this temperature for 14 hours. Afterward, the glass was air quenched at 600 °C before being

annealed at 190 °C for 4 hours. After synthesis, the glass was ground using a planetary ball mill in ambient lab conditions and sieved using a 200 mesh sieve in a MBraun glove box using a sieve shaker to prevent further exposure of powder with the ambient environment and to minimize moisture related impurities [10]. Particles with maximum dimensions ≤ 25 µm were then used to prepare the Fe^{2+}:ZnSe doped chalcogenide composite material.

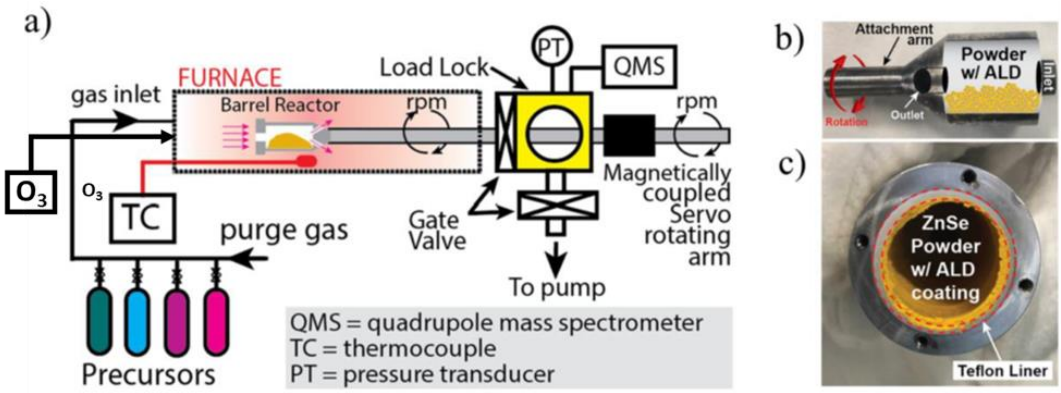

Figure 1. (a) Schematic of the ALD viscous flow reactor with updated in situ ozone generator. (b) cut-out figure of the barrel reactor with inlet/outlet attachment arm, (c) front view of the opened barrel reactor with coated ZnSe powder, adapted from [9].

2.3 Materials Characterization

The transmission data of parent glass and composite samples were evaluated via Fourier transform infrared spectroscopy (ThermoFisher Nicolet iS5 FTIR) with spectral resolution of 4 cm^{-1} and 32 accumulations. X-ray Diffraction (XRD) analysis of the parent glass and glass composite was measured using a PANalytical Empyrean basic X-ray diffraction system with a beam power of 1.8 kW, wavelength of $\lambda_{Cu\text{-}K\alpha}$ = 0.15418 nm, and current of 40 mA at room temperature. The XRD patterns of possible crystalline species were identified using Highscore software and the Joint Committee on Powder Diffraction Standards (JCPDS) PDF files of ZnS blende (No. 005- 0566) and ZnSe blende (No. 037-1463). XRD data have been normalized over the intensity value of the most intense peak. Moreover, to be representative and statistically meaningful, multiple images from several regions of various samples were recorded and the most characteristic results are presented here. A Zeiss Ultra 55 FEG Scanning electron microscopy was used to image crystallite shape and their dispersion throughout the surrounding glass matrix. ImageJ software was utilized to detect crystallites and extract their sizes in the SEM images.

Samples for transmission electron microscopy (TEM) were prepared by suspending the powders in alcohol via ultrasonication and depositing a drop of the suspension on a copper grid covered with a carbon film. The grid was air-dried for 15 min. High-resolution TEM (HRTEM) and Scanning TEM coupled with energy dispersive X-Ray spectroscopy (STEM-EDX) experiments were performed on a JEOL 2200 FS equipped with a field emission gun operating at 200 kV with a point-to-point resolution of 0.23 nm. High-resolution micrographs were acquired with a Gatan Ultrascan CCD 2kx2k camera and digital diffractograms were calculated with the Gatan Digital Micrograph software. Moreover, in order to be representative and statistically meaningful, multiple images from several regions of various samples were recorded and the most characteristic results are presented here.

3. RESULTS AND DISCUSSION

3.1 Morphology of dopant Fe^{2+}:ZnSe particles

The sizes of Fe^{2+}:ZnSe particles have been measured by coupling scanning and transmission electron microscopy techniques. Crossed analyses on the same sample were done due to the thickness limitation inherent to the TEM technique preventing observation of the whole particle. Figure 2(a) highlights the broad particle size distribution ranging from micrometers to several tens of micrometers. Figure 2(b) shows STEM used in bright field mode, giving the ability to characterize the smaller particles exhibiting similar contrasts to the one already observed during previous measurements. The alumina shell seems to be semi-continuous, as illustrated on Figure 2(c). Their thickness has been measured either directly from the SEM images or by processing STEM-EDX raw data. The mean thickness is about 40 nm, measured by plotting (Al+O) / (Zn+Se) concentration profiles and determining full-width half-maximum value as shown in Fig.2c.

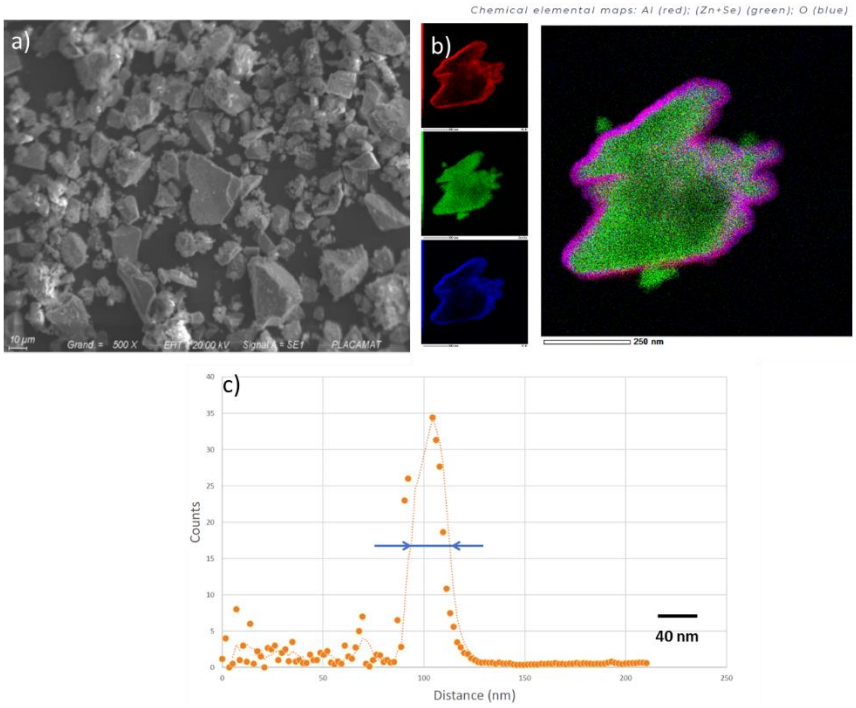

Figure 2a) Optical micrograph highlighting the broad particle distribution of the Fe^{2+}:ZnSe particles (scalebar 10 µm), b) STEM/EDS data illustrating the elemental map of the ALD alumina coating (pink) on Fe^{2+}:ZnSe particles, c) plot showing the measurement of mean thickness of alumina shell by determining the full width half maxima value of (Al+O)/(Zn+Se) concentration profiles.

To assess the post-remelt spatially dependent microstructure within the composite boule, slices of the composite from different locations within a 30 g boule (10 mm in diameter ampoule) (middle and bottom) were cut and polished for this work and discussed in the experiments below. The goal of this effort was to assess morphology of the composite, the extent of crystallite particle agglomeration and bubble content as a function of boule position, that would be representative of pre-forms to be used in subsequent fiber drawing experiments.

3.2 FTIR of composites

Figure 3 shows the FTIR spectra of different loading levels (0.5, 1.0 and 5.0 wt%) of Fe^{2+}:ZnSe loaded glass composite rods realized via the grinding melt/re-melt protocol. The FTIR spectra of the composites shown here correspond to the host glass and show a transmission wavelength cutoff of around 12 µm [9]. It is important to note that Fe^{2+}:ZnSe does not show a corresponding absorption band in the spectra, however absorption bands associated with adsorbed moisture on

unpurified starting materials are evident. As shown in Figure 3, the spectra of the middle and bottom positions indicate the same loading levels, ~~b~~being similar to each other, which confirms the uniformity of the composite within a boule. The presence of the As-O absorption band in the longwave 10.5 µm may have been derived from the powder handling [10].

As can be seen, there is a big difference between the transmission of 0.5 and 5 wt% loading level composites. This difference can be attributed to the Mie scattering caused due to the formation of Fe^{2+}:ZnSe aggregates, and the presence of bubbles with very different refractive index than that of the glass matrix, despite having a good theoretical refractive index match. Due to the interaction between the Fe^{2+}:ZnSe dopant particles with each other, they tend to come together and form aggregates inside the glass matrix. As the loading levels decrease (5.0 to 0.5 wt%), so the scattering losses reduce too, resulting in an increased transmission. Impurity absorption bands corresponding to -OH, H_2O, -S-H, CO_2,-Se-H, and -Se-O, were observed in spectra of the composites at 2.9 µm, 2.77 µm, 4.02 µm, 4.23 µm, 4.3 µm, 6.3 µm and 10.1 µm, respectively [13]. As the FTIR measurement was performed under atmospheric conditions the CO_2 and H_2O absorption bands can be attributed to the absorption by air. Despite the use of high purity raw materials and storage in a glove box under controlled environment, the presence of -OH, oxide and hydride impurities can be attributed to the handling of this material during the grinding and remelting steps.

Table 1 shows a summary of the relevant impurities observed to be present in the glass composite. Details of the impurity calculation protocol have been discussed [10]. To quantify the concentration of an impurity, the following relationship between absorption (α) and extinction coefficient (ε) can be used.

$$[Impurity] = \frac{\alpha(dB/m)}{\varepsilon(dB/m)} \quad (1)$$

Literature values of the extinction coefficients for -OH, -SH, and Se-H impurities can be seen in Table 1 along with the calculated absorption coefficients and concentrations in ppm. In our earlier work, a reduction in the impurity concentration was shown after the pre-heat treatment process of host glass and Fe^{2+}:ZnSe at 150 °C [10]. Maintaining a consistent drying protocol of 150 °C for 12 hours. resulted in reduction of OH impurity shown in Table 1.

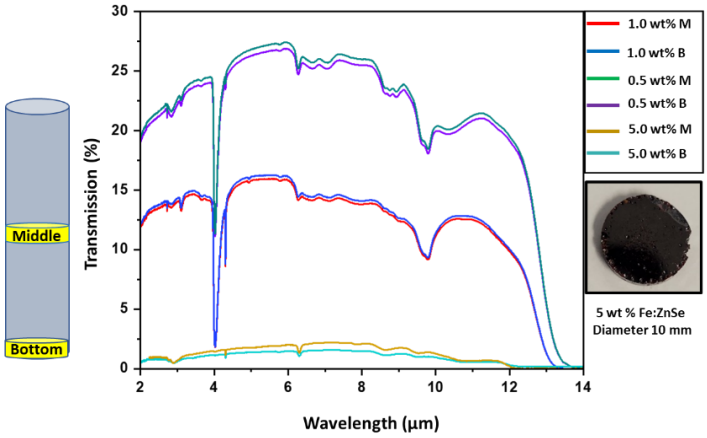

Figure 3. (left) Transmission spectra of the middle and bottom slices of the composite material made by different loading levels of Fe^{2+}:ZnSe doped As-S-Se ChG glass, each sample was ~ 1.5 (±0.6) mm thick. (Right) photograph of 5.0 wt% Fe^{2+}:ZnSe doped composite showing no visible

3.3 Phase identification of dopant particles

Figure 4 (a) shows the normalized XRD pattern of the host glass (no loading) with composites doped with 0.5, 1.0 and 5.0 wt% Fe^{2+}:ZnSe powders. A detailed comparison of ZnSe powder as reference in the host glass (94.6 As_2S_3 and 5.6 As_2Se_3) has been shown in our previous work [9]. The reference peaks of ZnSe at 27.2° (111), 45.23° (222), and 53.15° (311) peak are visible in all the slices. In addition to the ZnSe crystalline peaks, ZnS zincblende peaks (No. 005-0566) were also observed. The presence of ZnS is the sign of dissolution of ZnSe particles into Zn and Se and reprecipitation of Zn and S in the glass melt. While comparing the XRD data of the middle and bottom slices of the same loading levels GC, a higher volume fraction of ZnS was observed in the bottom slice as compared to the middle slice. This observation also supports the results shown in our previous work [8], that ZnSe powders have a tendency to settle down at the bottom of the melt in the melting ampoule, resulting in higher dissolution in the bottom slice as compared to middle slice.

Table 1: Relevant impurity concentrations of re-melted glass matrix with pre-heat treatment process of 150°C for 12 hr. under dynamic vacuum. The composite material was made by different loading levels of Fe^{2+}:ZnSe doped As-S-Se ChG.

Impurity	Position of the maximum of the absorption band (μm)	Extinction Coefficient, ε (dB/m · ppm)	0.5 wt%		1.0 wt%		5.0 wt%	
			α (dB/m)	[Impurity] ppm	α (dB/m)	[Impurity] ppm	α (dB/m)	[Impurity] ppm
H_2O	2.77	-	89.0	-	-		204	-
OH	2.90	5.0	300.24	60.04	320.69	64.13	310.56	62.22
SH	4.02	2.5	58.35	23.34	66	26.4	64.88	25.95
CO_2	4.23	-	34.4	-	-		44.5	-
Se-H	4.30	1.00	110.36	110.06	100.60	100.60	128.38	128.38

Our previous work [9] also showed ex-situ pre-coating of Fe^{2+}:ZnSe, due to the ozone pretreatment followed by ALD coating, which resulted in slower disssolution of Fe^{2+}:ZnSe in the host glass. In this work, the in situ oz pretreatment of the Fe^{2+}:ZnSe powders also gave rise to a slower dissolution, which was especially observed in 1.0 and 0.5 wt% loading level glass composites [9]. Figure 4 (b) shows evaluation of the volume fraction of ZnSe and ZnS crystallites in the bottom slice of the glass composites. The plot showed high volume fraction of ZnS (1.46%) in the bottom slice of 5 wt% doped composites as compared to 1.0 and 0.5 wt% composites (0.23% and 0.13%).

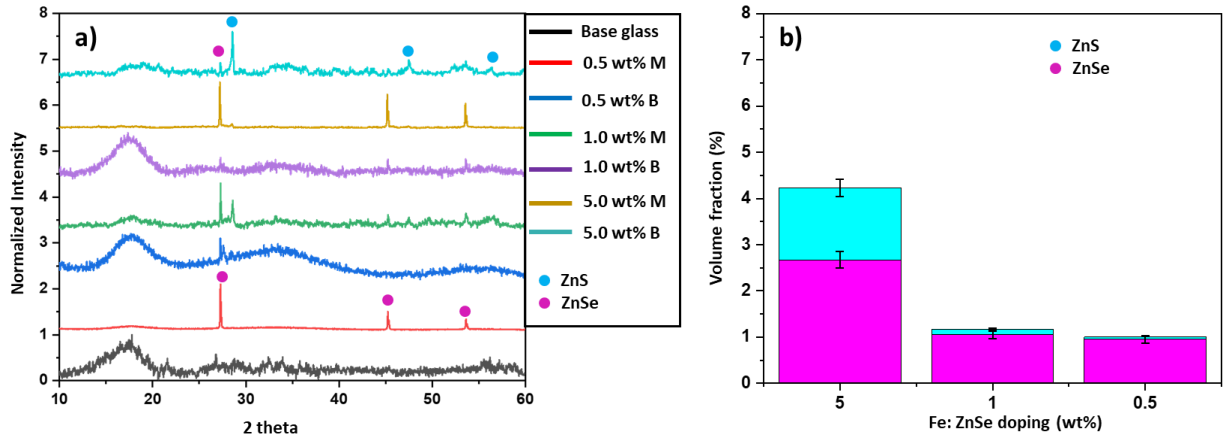

Figure 4. (a) Normalized XRD data of host glass, 0.5, 1.0 and 5.0 wt% Fe^{2+}:ZnSe doped glass composite, M and B represents middle and bottom position of the slice in the glass boule, (b) volume fraction of the ZnS and ZnSe crystals in the bottom slice of the 0.5, 1.0 and 5.0 wt% Fe^{2+}:ZnSe doped glass composite.

3.4 Aggregates in composites

The higher dissolution of the ZnSe into the host glass in the highly doped samples (5 wt%) compared to the lower (0.5 and 1.0 wt%) doped composites could be observed in Fig 5. First, there appears to be some ZnS present in the 0.5 and 1 wt% composites but it is likely below the detection limit of the XRD, therefore it cannot be precisely quantified.

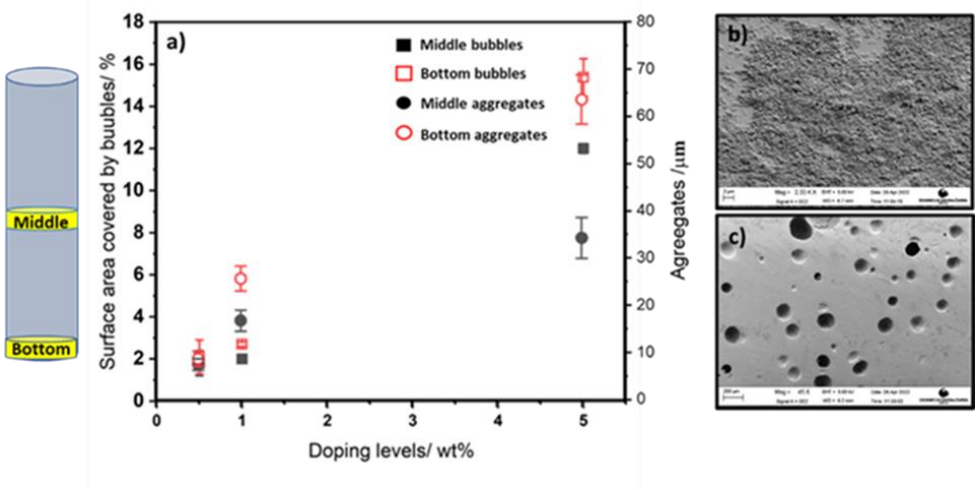

Figure 5 a) Plot showing a comparison between the surface area covered by bubbles and aggregates formed in the M and B slices of different loading levels. b) Optical micrograph (scalebar = 2 µm) depicting agglomerates of 64 (± 5.32) µm; c) Optical micrograph of slice taken from the bottom of the 5.0 wt% glass composite showing the large density of bubbles formed by which was believed to be associated with the partial dissolution of ZnSe to form ZnS (scalebar = 200 µm).

As discussed in our previous work [9], Fe^{2+}:ZnSe has a tendency to settle towards bottom of the ampoule when the host glass is melted. Maintaining a homogenous distribution of the Fe^{2+}:ZnSe particulates throughout the length of the ampoule has been a challenge in this work. In the case of high loading (5.0 wt%), when the Fe^{2+}:ZnSe particles came in contact with each other they formed aggregates. These aggregates tended to settle at the bottom of the glass ampoule. As can be seen in Figure 5a, composites with loading 5.0 wt% form aggregates with an average size of 64 (± 5.32) µm observed on the surface of the bottom slice as compared to 28 (± 3.12) µm and 10 (± 1.22) µm for the 1.0 and 0.5 wt% composites respectively. Similary, aggregates with an average size of 35.32 (± 4.00) µm, 18.16 (± 1.12) µm and 4.05 (± 0.56) µm were observed in the the middle slices of the composites from 5 wt%, 1 wt% and 0.5 wt% composites respectively. Figure 5b) shows SEM image of deposited aggregates on the 5 wt% doped bottom glass slice. The presence/ formation of large aggregates in the 5 wt% Fe^{2+}:ZnSe maybe the reason behind higher dissolution of ZnSe into ZnS, perhaps due to a build up of the dopant concentration and hence chemical potential.

Another observation via SEM image analysis is shown in Figure 5c, the composites had bubbles through out the surface, the bubbles were circular and deep. EDS analysis to identify chemical composition inside the bubbles was unsuccessful. The bubbles were too deep to focus the electron beam and get elemental composition. The sizes of the bubbles were measured using ImageJ software, as expected large aggregates in the 5 wt% composites also had associated large bubble ranging from 100 – 300 µm, covering ~ 16% of the sample surface with bubbles. On comparing with the low loading composites (1 and 0.5 wt%) samples, where 3% and 1.85% of the sample surface was covered with bubbles ranging 200-40 µm.

3.5 Photoluminescent emission from composites

The emission properties of bulk Fe^{2+} doped composites were measured using the experimental setup and protocol discussed in our previous work [11]. The fluorescence signal was measued at ~77 K, both as a function of time and wavelength and compared using a reference Fe^{2+}:ZnSe reference sample. Figure 6 (left) shows a comparison of the emission signal from two equally doped 5 wt% composites. Despite the composite's loss in the form of impurity absorption and bubble-related scatter loss, broadband emission covering the 3520-5200 nm spectral region was observed, indicating the presence of active Fe^{2+} ions. The new 5 wt% composites made via improved ALD and drying protocol showed higher emission signal with the same loading levels. Figure 6 (right) shows a comparison of the impurities concentrations in the old and new 5 wt% loading level samples. There are high concentrations of -OH and hydride impurities in the old 5 wt% composite. It is also important to understand that there are several factors that impact the emission signal strength including pump beam

quality, spot size, layout of the imagining system used to collect the fluoresecence signal, and sample orientaion. Best efforts were made to maintain the old experimental conditions.

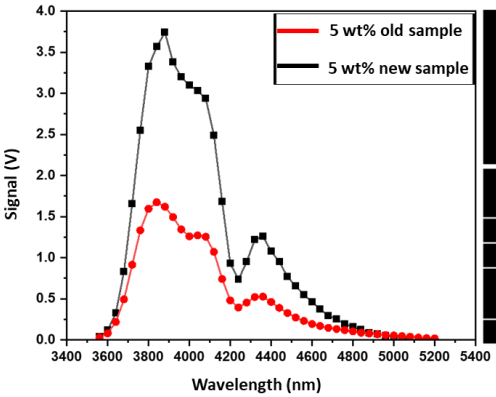

Impurity	Position of the maximum of the absorption band (μm)	Extinction Coefficient, ε (dB/m · ppm)	5.0 wt% (new sample)		5.0 wt% (old sample)	
			α (dB/m)	[Impurity] ppm	α (dB/m)	[Impurity] ppm
H_2O	2.77	-	204	-	456	-
OH	2.90	5.0	310.56	62.22	852.64	170.52
SH	4.02	2.5	64.88	25.95	78.25	31.3
CO_2	4.23	-	44.5	-	52.23	-
Se-H	4.30	1.00	128.38	128.38	156.25	156.25

Figure 6. (left) Shows a comparison of the measured fluorescence spectrum from the 5 wt% Fe^{2+}:ZnSe loaded composites (black) new bulk sample, (red) old equivalently loaded bulk sample, (right) Relevant impurity concentrations of re-melted glass matrix with 5 wt % loading levels old and new sample made without, and with pre-heat treatment at 150°C for 12 hr. under dynamic vacuum. Both the samples were ~ 1.5 (±0.6) mm thick.

The strong dip in the emission spectrum of both samples around 4.2 μm was due to absorption by atmospheric CO_2. The difference in CO_2 dip between both the samples can be explained via difference in path lengths through the atmosphere. As indicated in the XRD analysis, some of the ZnSe particles dissolved and recrystallized into ZnS. Fe^{2+} ions maybe substituting into ZnS crystals, but no spectroscopic evidence of the iron in the glass has been observed. The explanation of the recrsytallization of Fe^{2+} is still under investigation.

Despite high scattering loss in the composite material, incorporation of improved ALD coating and purification step (increased drying time) resulted in reduced impurity concentrations which further assisted in observation of higher emission signal making these results promising for future development of fiber laser sources opertaing at > 4 μm. Future efforts will focus on purification of starting materials, further drying, and use of other coatings to support the physical dispersion of particles to reduce agglomeration.

4. CONCLUSIONS

In this work composites were fabricated comprising Fe^{2+}:ZnSe microparticles dispersed in an index matched As-S-Se ChG glass matrix. Improved ALD on Fe^{2+}:ZnSe particles via in situ ozone generator and powder purification by means of extended drying in a tube furnace were applied to fabricate the composites. Fe^{2+}:ZnSe doped ChG composites were fabricated with loading levels, and a systematic study was done via XRD and image analysis using SEM and ImageJ on slices cut from different positions of the glass boule. The presence of aggregates and bubbles formed due to the aggregation and dissolution and reaction with ZnS dopant of ZnSe particles were quantified to the loading levels. As expected the composites with highest loading levels showed largest aggregates and bubbles compared to low loading levels of 1.0 and 0.5 wt% doped composites. In spite of agglomeration and bubble induced scattering losses, and host glass impurities; strong Fe^{2+} emission was observed which was higher than our previously reported work [11]. This is a promising step toward further improving the quality of ALD alumina shell coating by employing modifications in deposition conditions, as well as controlling the host glass -OH and hydride impurities by raw material purification.

Additional work is in progress where fibers are being drawn from the bulk composites of 0.5, 1.0 and 5 wt% composites. These results open the door towards fabrication of Fe^{2+}:ZnSe doped optical fibers, and work is on-going to quantify the Fe^{2+} emission in these optical fibers.

ACKNOWLEDGMENTS

We would like to acknowledge the initial work done by Dr. Matthew Chazot on this project, and Dr. Gary Cook at AFRL for providing the Fe^{2+}:ZnSe ceramic coupons. We would also like to acknowledge UGIEL for the characterization of Fe^{2+}:ZnSe particles via electron microscopy. This work was funded by AFOSR via the Grant FA9550-19-1-0127. This work was partially supported by the University of Central Florida under the preeminent Postdoctoral Program (P3).

REFERENCES

1. Xiolin, J., Soncompositeshoo, C., Yuanyuan, Y., Lianqing, Z., Wu. Y., Zhou, S. " Organic carbon prediction in soil cores using VNIR and MIR techniques in an alpine landscape," Sci. Rep., 7(1), 2144 (2017).
2. Waynant, R. W., Ilev L. K., Israel. G., "Mid–infrared laser applications in medicine and biology," Phil. Trans. R. Soc. A, 359(1789), 359635-359644 (2001).
3. Yiming, G., Yognian, G., Xusheng, Z., Chunqiu, Kelun, X., Lelu, H., Xiang, S., Zijun, L.," Development and characteristics of infrared gradient refractive index chalcogenide glasses by hot pressing," Opt. Express, 30(12), 21491-21500 (2022).
4. Jing, R., Xiaosong, L., Changgui, L., Jain, R. K., " Luminescent ion-doped transparent glass ceramics for mid-infrared light sources," Opt. Express., 28(15), 21522-21548 (2020).
5. Sorokin, E., Klimentov, D., Frolov, M. P., Korostelin, Y. V., Kozlovsky, V. I., Podmar'kov, Y. P., Skasyrsky, Y. K., Sorokina, I. T."Continuous-wave broadly tunable high-power Cr:CdS laser," App Phys. B, 117(4), 1009–1014 (2014).
6. Martyshkin, D., Kesterson, T., Fedorov, V., Mirov, S., "Mid-IR CW Cr:ZnS laser tunable with acousto-optical filter," Solid State lasers XXVI: Technology and Devices, 10082G (2017).
7. Fedorov, V. V., Mirov, B. S., Gallian, A., Badikov, V,. D., Frolov, P. M., Korostellin, V. Y., Kozlovsky, V. I., Landman, I. A., Podmar'kov, P. Y., Akimov, A., V., Voronov, A. A., " 3.77-5.05 μm tunable solid-state lasers based on Fe^{2+}- doped ZnSe crystals operating at low and room temperatures," IEEE Journal of Quantum Electronics, 42(9), 907-917 (2006).
8. Chazot, M., Arias, C., Kang, M., Blanco, C., Kostagiannes, A., Cook, J., Yadav, A., Rodriguez, V., Adamietz, F., Verreault, D., Danto, S., Loretz, T., Seddon, A., Furnis, D., Schepler, K., Richardson, C. M., Richardson, A. K., "Investigation of ZnSe stability and dissolution behavior in As-S-Se chalcogenide glasses," J. Non Cryst. Solids, 555, 120619 (2021).
9. Chazot, M., Kostagiannes, A., Julian. M., Feit, C., Sosa, J., Kang, M., Blanco, C., Cook, J., Rodriguez, V., Adamietz, F., Verreault, D., Banerjee, P., Schepler, K., Richardson, C. M., Richardson, A. K., " Enhancement of ZnSe stability during optical composite processing via atomic layer deposition," J. Non Cryst. Solids, 576, 121259 (2022).
10. Kostagiannes, A., Sharma, R., Howe, A., Chazot, M., Kang, M., Schepler, K., Richardson, A. K., " Role of powder handling on resulting impurities in ZnSe-doped As-S-Se composite materials," Opt. Mat. Express., 12(11), 4287-4298 (2022).
11. Cook, J., Chazot, M., Kostagiannes, A., Sharma, R., Feit, C., Sosa, J., Banerjee, P., Schepler, K., Richardson, C. M., Richardson, A. K., " Optically active Fe^{2+}-doped ZnSe particles in a chalcogenide glass matrix," Opt. Mat. Express., 12(4), 1555-1563 (2022).
12. Evans, W. J., Suites, W. R., Harris, R. T., " Increasing the performance of an Fe:ZnSe laser using a hot isostatic press," Opt. Mat. Express., 7(12), 4296-4303 (2017).
13. Sonopatin, G. E., Shriyaev, V. S., Plotnichenko, V. G., Dianov, M. E., Churbanov, F. M., " High-purity chalcogenide glasses for fiber optics," Inorg. Mater., 45(13), 1439-1460(2009).
14. Xiolin, J., Songchoo, C., Yuanyuan, Y., Lianqing, Z., Wu. Y., Zhou, S. " Organic carbon prediction in soil cores using VNIR and MIR techniques in an alpine landscape," Sci. Rep., 7(1), 2144 (2017).